Journal of Labelled Compounds and Radiopharmaceuticals

WILEY

Journal of Labelled Compounds and Radiopharmaceuticals

RESEARCH ARTICLE OPEN ACCESS

^{68}Ga Radiolabeling of NODASA-Functionalized Phage Display–Derived Peptides for Prospective Assessment as Tuberculosis-Specific PET Radiotracers

Christiaan A. Gouws[1] | Tricia Naicker[1] | Beatriz G. de la Torre[2] | Fernando Albericio[2] | Janie Duvenhage[3] | Hendrik G. Kruger[1] | Biljana Marjanovic-Painter[4] | Sipho Mdanda[3] | Jan R. Zeevaart[3,4,5] | Thomas Ebenhan[3,5] | Thavendran Govender[6]

[1]Catalysis and Peptide Research Unit, School of Health Sciences and School of Chemistry and Physics, University of KwaZulu-Natal, Durban, South Africa | [2]School of Chemistry and Physics, University of KwaZulu-Natal, Durban, South Africa | [3]Pre-clinical Imaging Facility (PCIF), Nuclear Medicine Research Infrastructure NPC, Pretoria, South Africa | [4]Radiochemistry, the South African Nuclear Energy Corporation (Necsa) SOC Ltd, Pelindaba, South Africa | [5]Department of Nuclear Medicine, University of Pretoria, Pretoria, South Africa | [6]Department of Chemistry, University of Zululand, KwaDlangezwa, South Africa

Correspondence: Thomas Ebenhan (thomas.ebenhan@up.ac.za) | Thavendran Govender (govenderthav@icloud.com)

Received: 27 May 2024 | **Revised:** 22 July 2024 | **Accepted:** 22 July 2024

Funding: The authors would like to thank their funders, the National Research Foundation (NRF) of South Africa (120419, 137961, and 145774), University of KwaZulu-Natal College of Health Sciences (UKZN-CHS), and Nuclear Medicine Research Infrastructure (NuMeRI, NPC) (PCI 2022-0012-A).

Keywords: imaging of infection | *Mycobacterium tuberculosis* | phage display | positron emission tomography | radiochemical characterization | radiolabeling

ABSTRACT

This research presents the development of positron emission tomography (PET) radiotracers for detecting *Mycobacterium tuberculosis* (MTB) for the diagnosis and monitoring of tuberculosis. Two phage display–derived peptides with proven selective binding to MTB were identified for development into PET radiopharmaceuticals: H8 (linear peptide) and PH1 (cyclic peptide). We sought to functionalize H8/PH1 with NODASA, a bifunctional chelator that allows complexation of PET-compatible radiometals such as gallium-68. Herein, we report on the chelator functionalization, optimized radiosynthesis, and assessment of the radiopharmaceutical properties of [^{68}Ga]Ga-NODASA-H8 and [^{68}Ga]Ga-NODASA-PH1. Robust radiolabeling was achieved using the established routine method, indicating consistent production of a radiochemically pure product (RCP ≥ 99.6%). For respective [^{68}Ga]Ga-NODASA-H8 and [^{68}Ga]Ga-NODASA-PH1, relatively high levels of decay-corrected radiochemical yield (91.2% ± 2.3%, 86.7% ± 4.0%) and apparent molar activity (A_m, 3.9 ± 0.8 and 34.0 ± 5.3 GBq/μmol) were reliably achieved within 42 min, suitable for imaging purposes. Notably, [^{68}Ga]Ga-NODASA-PH1 remained stable in blood plasma for up to 2 h, while [^{68}Ga]Ga-NODASA-H8 degraded within 30 min. For both ^{68}Ga peptides, minimal whole-blood cell binding and plasma protein binding were observed, indicating a favorable pharmaceutical behavior. [^{68}Ga]Ga-NODASA-PH1 is a promising candidate for further in vitro/in vivo evaluation as a tuberculosis-specific infection imaging agent.

1 | Introduction

Tuberculosis (TB) is an infectious disease caused by the pathogen *Mycobacterium tuberculosis* (MTB) and poses a global health concern because it is one of the leading causes of global infectious disease deaths in 2021, accounting for up to 1.6 million reported deaths [1]. More concerning, due to recent COVID-19–related healthcare disruptions, a net resurgence of MTB

infection incidence and mortality rates occurred after more than a decade of consistent annual decline. This made infection-related Sustainable Development Goals (SDGs), which set out for a 90% reduction in TB deaths by 2030, realistically unattainable [2]. Additionally, the continuous emergence and spread of drug-resistant MTB infections pose a significant threat to global health and development [2].

Positron emission tomography (PET) imaging has become an emerging, elegant tool for the diagnosis or monitoring of intricate bacterial infections [3]. Its ability to detect infections through noninvasive whole-body scans is of great value in cases of deep-seated and occult infections [4, 5]. PET achieves this by visualizing infection-related molecular processes through quantitative measurements of target site–specific radiotracer accumulation. This ability also makes it an efficient research tool for treatment optimization and drug development efforts [6, 7].

Radiotracers are typically biologically active molecules that are designed to accumulate at a certain biochemical or (sub)cellular target, which are radiolabeled or tagged with a PET-compatible radionuclide (i.e., a radionuclide that emits a positron upon decay) [8]. Radiolabeling strategies of these biomolecules involve covalent linkage of, for example, either fluorine-18 ($t_{1/2} = 110$ min) or carbon-11 ($t_{1/2} = 20$ min) but also the use of bifunctional chelators for chemical complexation of metal-based radioisotopes (gallium-68, $t_{1/2} = 68$ min or copper-64, $t_{1/2} = 12.7$ h) [8, 9].

Currently, the "gold-standard" PET imaging agents for the assessment of bacterial tissue manifestations include 2-deoxy-2[^{18}F]F-D-glucose ([^{18}F]FDG) and radiolabeled white blood cells (e.g., [^{111}In]In-WBC). However, these methods lack specificity towards bacteria, as uptake is not based on a direct interaction with bacterial pathogens, but rather on secondary host-mediated inflammatory responses, and are therefore nonspecific for infection [10–12]. The resulting limitations associated with these radiotracers in infection imaging have been well documented [11, 13–15]. Thus, PET imaging alone is not able to fully diagnose all aspects of the infection, and more conventional investigations, such as fluid analysis, tissue biopsies, and bacterial culturing, need to be utilized for sufficient diagnosis [5, 7, 11].

To this end, the development of desired radiotracers capable of distinguishing between infection and sterile inflammation, as well as the causative species of bacteria (such as MTB), has become highly feasible, not only for direct and differential diagnosis of infection but also for managing and monitoring patients' responses to therapy and experiments concerning the development of new antimicrobials [5, 16–18]. Additionally, in light of the increasing emergence of highly drug-resistant TB, early detection and identification of MTB are crucial to ensure optimal antimicrobial treatment interventions before the onset of major tissue damage and formation of caseous granulomas, which are notoriously difficult to treat [19, 20]. To our knowledge, no clinically approved radiotracer showed evidence of specific binding to MTB over other bacterial species in vivo [21]. Thus, the design and development of novel radiotracers, specifically for the selective diagnosis of bacterial infections, particularly MTB, are warranted.

Phage display technology offers a powerful platform for the discovery and engineering of peptides with specific binding properties [22]. This technology involves the genetic engineering of bacteriophages to create a library of phages that express foreign peptides on their surfaces. In this library, phages that bind entire MTB cells can be selected and isolated through directed evolution by repeated exposure to the target, followed by isolation and propagation cycles [22]. As reported, two phage display–derived peptides with proven specific binding to MTB cells were identified, thereby serving as radiotracer vector scaffolds for development as MTB-specific PET nuclear imaging agents.

The first peptide, designated H8 (core sequence WHSGTPH), is a linear peptide with evidence of selective binding capabilities to the MTB H37Rv reference strain [23]. After four rounds of biopanning against MTB H37Rv whole cells, five unique peptide sequences were obtained, of which H8 showed the highest affinity. H8 was chemically synthesized in its native and biotinylated forms with a flexible linker peptide added to the N- or C-terminal ends. The peptide was then evaluated for its binding affinity and specificity to H37Rv and other bacteria. The measured disassociation constant of H8 for MTB H37Rv showed a significantly stronger binding affinity as opposed to BCG vaccine, *Pseudomonas aeruginosa*, and *Escherichia coli*. By functionalizing magnetic microspheres (MMSs) and quantum dots (QDs) with H8, the authors could detect 10^3 colony-forming units (CFU)/mL MTB H37Rv cells in sputum samples based upon the formation and concentration of a sandwich complex composed of bacterial cells, MMSs, and QDs (MMS-H8 + bacteria + QD-H8).

The second peptide, designated PH1 (with a core sequence of CPLHARLPC), is a cyclic peptide that demonstrated selective binding capabilities to various mycobacteria [24]. It was discovered through the process of biopanning a library of phages against immobilized whole cells of a nonpathogenic strain of MTB (Dleu/Dpan). PH1 was identified as the most prevalent clone after five rounds of biopanning as determined by high-throughput sequencing, which revealed that it accounted for > 80% of the sequenced population. PH1 was found to specifically bind mycobacteria by ELISA and surface plasmon resonance experiments. This includes two strains of MTB (H37Rv and Dleu/Dpan), *Mycobacterium bovis* BCG and *Mycobacterium smegmatis*, but did not significantly bind to other unrelated pathogenic bacteria such as *E. coli*, *Corynebacterium xerosis*, *Streptococcus pyogenes*, or *Staphylococcus aureus*. Additionally, it was found that PH1 binds to a 15-kDa protein detected in whole-cell lysates of MTB, which was not detected in the lysate treated with protease. However, the identity of this protein has not yet been determined.

We sought to functionalize H8 and PH1 with 1,4,7-triazacyclononane-1-succinic acid-4,7-diacetic acid (NODASA), a bifunctional chelator that enables efficient capture of radiometals such as radioactive gallium-68 [25, 26]. In general, the half-life of gallium-68 (68 min) makes it suitable for peptide pharmacology [27]. Additionally, ^{68}Ga activity can be acquired from ^{68}Ge/^{68}Ga generators, a cheaper and more accessible option than cyclotron-produced radionuclides, which is important for resource-limited countries where TB is more prevalent. Herein, we report the successful conjugation of NODASA to H8 (NODASA-H8) and PH1 (NODASA-PH1) peptides using

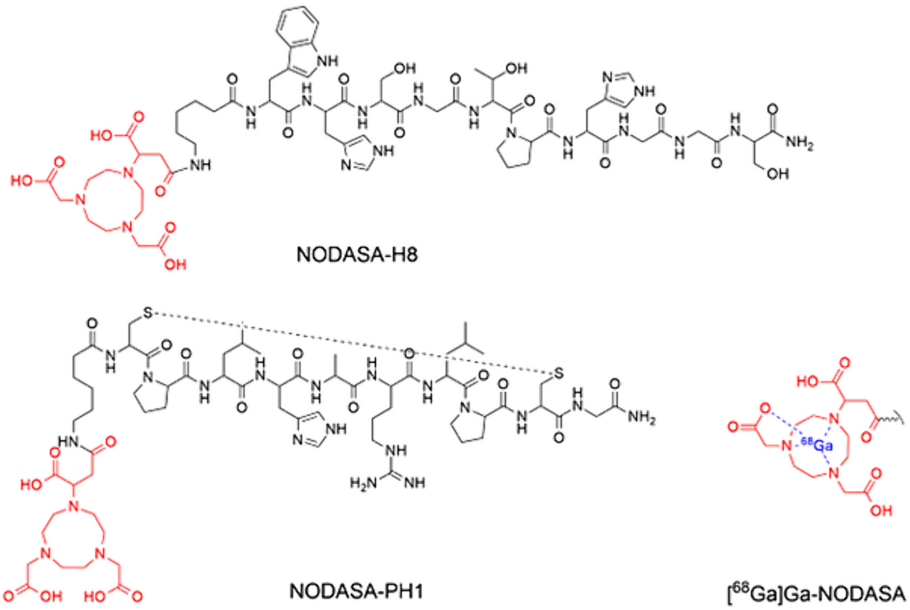

FIGURE 1 | Chemical structures of 1,4,7-triazacyclononane-1-succinic acid-4,7-diacetic acid (NODASA)-functionalized H8 (NODASA-H8; linear peptide) and PH1 (NODASA-PH1; cyclic peptide) synthesized by solid-phase peptide synthesis (also see the Supporting Information).

an on-resin solid-phase peptide synthesis method previously published by Dutta et al. [28]. This was followed by the development and optimization of ^{68}Ga radiosyntheses to introduce the radiotracers [^{68}Ga]Ga-NODASA-H8 and [^{68}Ga]Ga-NODASA-PH1 to initial radiopharmaceutical characterization (Figure 1). As the first investigative milestone, the outcome for this study may be indicative of whether [^{68}Ga]Ga-NODASA-H8 and/or [^{68}Ga]Ga-NODASA-PH1 may be justified tracers for further mycobacterial testing and preclinical assessment as prospective radiotracers for PET imaging of TB infection.

2 | Experimental

2.1 | Peptide Design

The following modifications to the peptide core sequences were applied: (H8) based on original work [23], a structurally flexible GGS cap was added to the C-terminal domain of the peptide to maintain functional confirmation; (PH1) a glycine was added to the C-terminal of the peptide to circumvent unwanted side reactions associated with loading resin with cysteine, such as epimerization [29]. For ease of synthesis and to potentially enhance in vivo stability, C-terminal domain amination was applied to both the peptides. The NODASA conjugation was carried out on the N-terminal peptide domain using 6-aminohexanoic acid as a linker and spacer to ensure that the peptide's functional conformation was preserved with minimal interference from the NODASA chelator.

2.2 | Peptide Synthesis and NODASA Conjugation

9-Fluorenylmethoxycarbonyl (Fmoc)-Rink amide resin, Fmoc-protected L-amino acids, and coupling reagents were purchased from GLS Biochem Systems, Inc. (China). All the chemicals and reagents were purchased from Sigma-Aldrich (United States), DLD Scientific (South Africa), and Hangzhou Dayang Chemical Co. Ltd. (China). All solvents used for the synthesis and purification of the peptides were of high-performance liquid chromatography (HPLC) grade and were purchased from Sigma-Aldrich. All synthetic steps were characterized using a PDA-coupled ESI-LCMS (Shimadzu, Japan) mounted with a YMC-Triart C18 (5 μm, 4.6 × 150 mm) column (YMC Co., LTD, Japan) to calculate their purities and identify their respective masses.

Peptides were manually synthesized on a 0.2-mmol scale using standard Fmoc/*tert*-butyl (tBu)–solid-phase peptide synthesis protocols. The peptides were synthesized on a rink amide resin with a loading value of 0.52 mmol/g. OxymaPure and *N*,*N*′-diisopropylcarbodiimide (DIC) were used as activator/coupling reagents. Equal molar concentrations of Fmoc-amino acid, OxymaPure, and DIC (1:1:1) dissolved in DMF (2.0 mL) were used in a cocktail for each coupling cycle. An excess of 5 equivalents (equiv.) of Fmoc-amino acid cocktail was used for initial resin loading, followed by 3 equiv. for subsequent coupling reaction cycles. Fmoc deprotection between each coupling cycle was achieved by suspension in 5.0 mL of 20% piperidine in DMF for 10 min. The resin was washed with 2 × 5.0-mL DCM and 2 × 5.0-mL DMF after each coupling and deprotection cycle, respectively. The completion of the reactions was monitored using the coulometric ninhydrin test [30].

On-resin NODASA conjugation was performed according to a procedure developed by Dutta et al. [28]. Briefly, 3-(4,7-bis(((9*H*-fluoren-9-yl)methoxy)carbonyl)-1,4,7-triazonan-1-yl)-4-methoxy-4-oxobutanoic acid (an Fmoc-protected NODASA precursor) was first synthesized off the resin and then coupled to the amino terminus of the already-synthesized peptide on the resin by the addition of a reaction mixture containing a 1:1:1 ratio of precursor (3.0 equiv.):DIC (3.0 equiv.):OxymaPure (3.0 equiv.) dissolved in DMF (1.0 mL) for 2 h. Once coupled on the resin, Fmoc deprotection was

carried out (5.0 mL of 20% piperidine, 10 min), exposing the secondary amines on the NODASA core. These were substituted with tBu bromoacetate (3 equiv.) in the presence of *N*,*N*-diisopropylethylamine (DIPEA, 3 equiv.) dissolved in 2.0 mL of *N*-methyl-2-pyrrolidone with a reaction time of 30 min. Finally, hydrolysis of the methyl ester on one of the NODASA chelator arms was achieved on the resin by treatment with 5 mL of 1:1 THF-MeOH (v/v) for 2 × 15 min. Peptide cleavage from the solid support and the simultaneous removal of all protecting groups were carried out by treating the resin-bound peptide with a 95:5 mixture (v/v) of TFA/H_2O (2.0 mL/0.1-mmol scale) for 4 h at 50°C, followed by filtration. TFA was evaporated with the aid of N_2-gas bubbling until 0.5–1.0 mL remained. Peptide products were precipitated in diethyl ether (5.0 mL) and then centrifuged at 10,000 rpm for 5 min, after which the diethyl ether was decanted. After two additional diethyl ether washes, the resulting precipitate was dried under vacuum to remove residual diethyl ether. HPLC and LCMS analyses were performed to determine the purity and confirm the correct mass of the final peptide products.

2.3 | NODASA-PH1 Cyclization

The cyclization reaction, by disulfide bond formation between the two cysteine residues, was performed using the method described by Calce et al. [31]. The crude peptide was dissolved in 0.05 M of NH_4HCO_3 solution in water (final concentration of 0.4 mg/mL of peptide, at pH 7–8) and stirred vigorously in an open atmosphere to promote the oxidation reaction. Cyclization progression was monitored using LCMS. After 48 h (> 85% cyclization was achieved), the reaction mixture was acidified with acetic acid to pH 4 and freeze-dried. The cyclized product was purified by semipreparative RP-HPLC.

2.4 | Peptide Purification

Crude peptide products were purified using a semipreparative RP-HPLC system (Shimadzu, Kyoto, Japan) coupled to an ACE C18 preparative column (150 × 21.2 mm) using 0.1% TFA in water as Mobile Phase A and 0.1% TFA in acetonitrile as Mobile Phase B, with a flow rate of 10 mL/min. For NODASA-H8 purification, a gradient of 15%B–20%B within 20 min was used; for cyclized NODASA-PH1, a gradient of 5%B–50%B within 25 min was used. PDA detection was set at 220 nm. The collected fractions were characterized by LCMS identification of the desired product *m*/*z* (M+2H: NODASA-H8 = 739.1 *m*/*z*; cyclized NODASA-PH1 = 760.1 *m*/*z*) and fraction purity. Fractions with purity >95% were combined, followed by removal of residual acetonitrile in vacuo and freezing at −80°C. Subsequent freeze-drying yielded a white powder.

2.5 | Preparation of Nonradioactive Ga-NODASA-H8 and Ga-NODASA-PH1 Reference Compounds

Peptides were complexed with nonradioactive gallium(III) chloride as follows: 200 μL of 20 mM $GaCl_3$ dissolved in 0.6 M HCl was diluted with 400 μL 0.6 M HCl and mixed with 240 μL of a 2.5 M sodium acetate solution (pH 4–5). Next, 100 μL of 20.0 mM NODASA-PH1 or NODASA-H8 (0.5 equiv. to Ga) was added, followed by incubation at room temperature for 15 min. Ga-NODASA-H8 and Ga-NODASA-PH1 *m*/*z* confirmation and purity were analyzed using a LCMS (Agilent Technologies Inc., Wellington, DE, USA) coupled with a diode array detector (DAD) using both methods specified in Table 1.

2.6 | Gallium-68 Radioactivity Production and [^{68}Ga]Ga^{3+} Preparation

A tin dioxide germanium-68 (^{68}Ge)/(^{68}Ga) generator initially loaded with 1.85 GBq of ^{68}Ge activity was maintained daily by eluting radioactive material using 10 mL of 0.6 M HCl solution. For radiolabeling, ^{68}Ga activity was acquired by an eluate fractionation method [32]; the first 1.0 mL of eluate was discarded into a waste vial, while the next 2.0 mL, which contained the majority of the ^{68}Ga activity, was collected and saved in a separate vial for use in radiolabeling reactions. The generator line was then rinsed with the remaining 7.0 mL into the waste vial. The radioactivity of both the eluate and waste fractions was measured using a CRC Capintec 15 beta dose calibrator (CM Nuclear Systems, Orange Grove, Johannesburg, RSA). The ^{68}Ga eluate was then buffered to the appropriate pH using 2.5 M sodium acetate trihydrate and, without further purification, used for radiolabeling experiments.

TABLE 1 | Respective radio-HPLC methods used to analyze [^{68}Ga]Ga-NODASA-H8 and [^{68}Ga]Ga-NODASA-PH1 radiochemical purity (%RCP).

Method	Column	Mobile phase	Flow (mL/min)	Gradient/ time	Free ^{68}Ga species R_T (min)	Labeled ^{68}Ga peptide	R_T (min)
1	Poroshell 120, EC-C18, 3.0 × 150 mm; 2.7 μm	A: H_2O (0.1% TFA)	0.5	5%B–60%B in 15 min	1.32–2.40	[^{68}Ga] Ga-NODASA-H8	6.69
		B: acetonitrile (0.1% TFA)				[^{68}Ga]Ga-NODASA-PH1	8.32
2	Zorbax SB C-18 4.6 × 250 mm, 5 μM	A: H_2O (0.1% TFA)	1.0	5%B–60%B in 15 min	2.20–3.80	[^{68}Ga] Ga-NODASA-H8	8.35
		B: acetonitrile (0.1% TFA)				[^{68}Ga]Ga-NODASA-PH1	9.95

2.7 | Radio-HPLC Methods for Characterization and Radio Analysis Radiolabeled Peptides

Two distinct radio-HPLC systems and their respective methods were used to assess the radiochemical purity (%RCP) of radiolabeled products for logistical reasons (Table 1). The Agilent 1200 series (System 1) and the Agilent 1260 Infinity II (System 2) HPLC instruments, both equipped with a DAD set at 220 nm and a radioactive detector (Sockel 2 GABI Nova, Raytest, Straubenhardt, Germany), were used for radio analysis. Samples were injected without prior purification, and those containing ethanol were thoroughly dried and resuspended in water to prevent significant changes in retention time (R_T) and peak shape. After the gradient, a wash phase consisting of 95% acetonitrile was carried out for 5 min, followed by 5 min of re-equilibration.

2.8 | Characterization of Radiolabeled Peptides

For ^{68}Ga-labeled peptide characterization, initial radiolabeling of NODASA-H8 and NODASA-PH1 was performed using a ligand concentration of 100 μg/mL at room temperature for 20 min using generator-produced, buffered ^{68}Ga activity prepared as previously described. Radio characterization was performed using radio-HPLC Method 1.

To confirm the identity of the ^{68}Ga-labeled peptides, we first analyzed nonradioactive reference standards of each peptide (labeled with isotopically stable gallium) using LCMS (Agilent Technologies Inc., Wellington, DE, United States) with a DAD using the same HPLC method. We confirmed the identity of the nonradioactive Ga peptide peaks through observed m/z values. Then, we confirmed the identity of the radioactive ^{68}Ga peptides by comparing peak R_Ts observed on the radiochromatogram with the peak R_Ts observed on the UV chromatogram of the nonradioactive Ga peptide reference standards.

2.9 | ITLC Radio Analysis

Two ITLC methods were used to calculate the radiochemical yield (%RCY) of the crude product and assess radiotracer stability. Method 1 was used to determine the %RCY of both peptides as described by Ebenhan et al. [33]. Briefly, 15.0-cm impregnated silica gel (ITLC-SG) paper strips were spiked 1.0 cm from the bottom with 2 μL of ^{68}Ga peptide solution and then developed in a mixture of 1.0 M ammonium acetate/methanol 1:1 (v/v) as the mobile phase. The calculated R*f* values is 0.20 for ^{68}Ga colloids and free unreacted ^{68}Ga species, versus 0.69 for [^{68}Ga]Ga-NODASA-H8 or 0.70 for [^{68}Ga]Ga-NODASA-PH1.

In Method 2, a 0.1 M citrate solution (pH 5.0–5.5) was used as the mobile phase to determine the percentage of free unreacted ^{68}Ga species. For [^{68}Ga]Ga-NODASA-H8, the calculated R*f* values is 0.28 (+^{68}Ga colloids) versus 0.82 for free ^{68}Ga. For [^{68}Ga]Ga-NODASA-PH1, the calculated R*f* value is 0.24 (+^{68}Ga colloids) versus 0.79 for free ^{68}Ga. EDTA transchelation was also assessed using this method, with [^{68}Ga]Ga-EDTA showing an R*f* value of 0.65 [33]. The ITLC strips were dried and analyzed on an ITLC scanner system (miniGITA, Raytest, Germany) coupled with a gamma radiation detector to obtain ITLC chromatograms. Examples of each ITLC method's chromatogram is displayed in Figures S8–S10.

2.10 | Development and Evaluation of Optimal Radiolabeling Parameters

The reaction series were performed in Eppendorf 1.5-mL plastic tubes. Appropriate peptide concentrations were prepared using a series of stock dilutions, of which 25 μL was mixed with 225 μL of buffered ^{68}Ga solution (~50.0 MBq, pH 3.5–4.5) and incubated in a water bath. Peptide stocks and buffers used in this experiment were prepared using metal-free Millipore (deionized) water. The selection of pH 3.5–4.5 was based on NOTA-based radiolabeling recommendations from the literature, citing a pH between 3 and 5 as essential [25, 34]. A set of maximum 12 reactions was performed from a single gallium generator elution; every data point represents an independent reaction. The %RCY of each reaction product was monitored using ITLC Method 1.

The stability of both the peptides and radiometal conjugate was evaluated through a radiolabeling reaction that was incubated for up to 25 min at 80°C, followed by radio-HPLC analysis (Method 1) to determine the quantity of intact ^{68}Ga peptide, free ^{68}Ga, and degraded ^{68}Ga peptide (appearance of additional unknown radio-HPLC peaks). A sample for radio-HPLC analysis was taken at 5 and 25 min. Radioligand concentrations of 75 μg/mL for NODASA-H8 and 25 μg/mL for NODASA-PH1 were used.

2.11 | Radiopeptide Purification

Purification of crude [^{68}Ga]Ga-NODASA-H8/-PH1 products was achieved using a method described by Ebenhan et al. [33]. Briefly, this method utilized Sep-Pak light C18 (130 mg, Waters Corp., Milford, United States) SPE cartridges, which were preconditioned with 2.0 mL of EtOH, followed by 2 × 5.0 mL of Millipore deionized water. The crude peptide samples were loaded onto the cartridges with a flow rate of 2.0 mL/min, followed by 1.0 mL of water to rinse the reaction vial and transfer the residual ^{68}Ga-labeled peptide. The cartridges were then rinsed with 5.0 mL of water to remove any residual unbound ionic $^{68}Ga^{3+}$. Desorption of both ^{68}Ga-labeled peptides was achieved using 2.0 mL of 1:1 ethanol/water (v/v). All steps of the purification were run dry, and the ethanol was evaporated from the final product with gentle heating under pressurized airflow. The product fraction was analyzed using radio-HPLC (System 2) to calculate %RCP. The activity of both the cartridge and elution volumes was also measured after each applied treatment using a CRC Capintec 15 beta dose calibrator to monitor the desorption of the radiolabeled product from the SPE cartridge. If required, the ^{68}Ga peptide solutions were sterile filtered through a 0.22-μm membrane using a Millex, low–protein-binding filter (Millipore, Midrand Johannesburg, South Africa) before application.

2.12 | Evaluating the Radiolabeling Performance of the Optimized Radiosynthesis Protocol

The proposed optimized radiosynthesis protocol was employed multiple times for radiolabeling, incorporating SPE purification

to assess key performance parameters. The radiosynthesis process was carried out in 10-mL clear borosilicate glass vials. To compare the two peptides, we equally split the originally eluted ^{68}Ga activity (2.0 ± 0.2 mL). Thus, the maximum volume of 1.0-mL buffered gallium was used. To determine the %RCP for both the crude and final SPE-purified radiolabeled products, radio-HPLC (Method 2) was employed. The activity involved before and after each radiosynthesis and SPE purification step was measured using a CRC Capintec 15 beta dose calibrator to calculate radiochemical yield (%RCY), recovered activity (%), and activity loss to apparatus including ^{68}Ga colloids (%). The measured activity fractions were corrected for decay to the time when the crude radiolabeled product was loaded onto the SPE cartridge.

2.13 | Challenge and Stability Studies

The stability of [^{68}Ga]Ga-NODASA-H8/-PH1 in terms of ^{68}Ga chelation was examined using conditions outlined by Dutta et al. [35]. To begin, crude radiolabeled peptide product samples were suspended in buffered reaction solution (referred to as benchtop stability), in 0.1 M PBS (pH 7.4), or in the presence of 50-, 100-, and 1000-fold excess EDTA (adjusted to pH 7.4 using 1.0 M NaOH) and were incubated at either room temperature for up to 180 min (benchtop) or 37°C for up to 90 min (PBS and EDTA). For PBS and EDTA stability samples, 100 μL of ^{68}Ga peptide was added to 100 μL of PBS or 100 μL of EDTA solution. The change in percentage (%) of ^{68}Ga peptide integrity was monitored over time using ITLC. Samples of benchtop and PBS were analyzed using the 1.0 M ammonium acetate/methanol 1:1 (v/v) ITLC method to determine the quantity of intact ^{68}Ga peptide normalized to the %RCP of the radiolabeled peptide product used for the challenge. Samples of EDTA stability were analyzed using the 0.1 M citrate solution (pH 5.0–5.5) ITLC method to quantify the emergence of free ^{68}Ga and ^{68}Ga-EDTA species.

2.14 | Physicochemical Characterization ($LogD_{7.4}$)

The lipophilicity of [^{68}Ga]Ga-NODASA-H8/-PH1 was determined using the *n*-octanol/PBS (pH 7.4) system test as described by Shi et al. [36]. Radiochemically pure (> 98%) radioconjugate was produced using the routine radiolabeling procedure, followed by dilution with PBS to achieve pH 7.4. For the test, 1.0 mL of radioconjugate/PBS solution (~12 MBq) was added to 1.0 mL of *n*-octanol and vortexed for 2 min. The mixture was separated into separate layers by centrifuging at 4500 rpm for 5 min. An aliquot of 900 μL of each layer was transferred into separate Eppendorf tubes. The activity of each phase was determined using a well type of CRC Capintec 15 beta dose calibrator and used to calculate $LogD_{7.4}$. The $LogD_{7.4}$ of each sample ($n = 3$) was calculated as $Log(k_{o/w})$, the logarithm of the ratio of decay-corrected activity between the octanol and water layers ($k_{o/w}$). The results are represented as average ± SD.

2.15 | Proteolytic Stability and Blood Distribution Assays

Blood samples were obtained through the use of heparinized vacutainer tubes, which were graciously provided by the Nuclear Medicine Research Department at the University of Pretoria. These samples were kept on ice until they were needed for further use. Plasma samples were collected through centrifugation at 4000 rpm for 2 min using a LCEN-401P digital clinical centrifuge manufactured by MRC Laboratory Equipment (Harlow, United Kingdom).

For all experiments, the vials containing blood, plasma, or serum were preheated to 37°C for 5 min before the addition of the ^{68}Ga peptide. Both ^{68}Ga peptides were prepared by using the optimized radiosynthesis procedure (see previous methods herein) and had an RCP of > 95%. Before being added to plasma, the pH of the radiolabeled products was adjusted to 7.0–8.0 using 1.0 M NaOH. The assays were performed using sterile Eppendorf tubes.

The plasma stability of both peptide radioconjugates was investigated using a method described by Xia et al. [37]. ^{68}Ga peptide (~10 MBq) was added to 1.0 mL of plasma and incubated at 37°C. At time points $T = 5$, 30, 60, and 120 min, a 200-μL aliquot was taken and mixed with 1.0 mL of ice-cold ethanol to precipitate plasma components. The resulting suspension was separated by centrifugation at 4500 rpm for 5 min, and an aliquot of 100 μL of the supernatant was collected for radio-HPLC determination of radiochemical integrity. Before injection, the sample was prepared by evaporation of methanol and resuspension in 100 μL of water. Stability was assessed using radio-HPLC (Method 1) by calculating the %RCP relative to the administered radioconjugate %RCP.

The blood cell association of both peptide radioconjugates was investigated by the method described by Shi et al. [36]. In brief, either [^{68}Ga]Ga-NODASA-PH1 or [^{68}Ga]Ga-NODASA-H8 (~5.0 MBq in 100 μL) was mixed with 1.2 mL of heparinized whole blood. The mixture was incubated in a shaking incubator at 37°C. At $T = 0$, 30, and 60 min, a blood aliquot of 300 μL was transferred to a yellow-cap BD Vacutainer (containing a clot activator/polymer gel) (BD Diagnostics, Franklin Lakes, United States). These tubes were then centrifuged at 4500 rpm for 2 min to separate the serum from the blood cells, which were absorbed into the gel layer. The serum was rinsed into a separate tube using PBS (2 × 0.5 mL). The serum and blood cells were measured separately using an automated gamma counter (Hidex AMG, Turku, Finland). The blood cell association was calculated by dividing the total radioactivity measured in the blood collection tube by the combined activity of both tubes. The experiment was repeated three times, and data are presented as average ± SD. Statistical significance between timepoints was calculated using a two-tailed *t*-test, and a $p < 0.05$ was considered significant.

The protein-binding assay was done as described by Mdlophane et al. [38]. In brief, [^{68}Ga]Ga-NODASA-PH1 or [^{68}Ga]Ga-NODASA-H8 (~1.5 MBq in 20 μL) was mixed with 500 μL of plasma. The mixture was incubated in a shaking incubator at 37°C. At $T = 0$, 30, and 60 min, an aliquot of 100 μL was taken for sample processing. Proteins were precipitated in ice-cold ethanol (500 μL) and centrifuged (4500 rpm, 10 min). The supernatant was removed, and the protein pellet was washed twice with another 500 μL of ethanol. The washed protein pellets and supernatants were measured in an automated gamma counter

(Hidex AMG, Turku, Finland). The percentage of labeled compound that was bound to plasma protein was determined by distribution ratio between the protein pellet and supernatant. The experiment was repeated three times, and data are presented as average ± SD. Statistical significance between timepoints was calculated using a two-tailed *t*-test, and a $p < 0.05$ was considered significant.

3 | Results and Discussion

3.1 | NODASA-H8 and NODASA-PH1 Synthesis

On-resin synthesis and conjugation of H8 and PH1 to NODASA (using 6-aminohexanoic acid as a linker) were successful using the SPPS method adapted from Dutta et al. [28], with yields of 90.7% for NODASA-H8 and 91.1% NODASA-PH1. After cleavage from the resin, NODASA-PH1 was successfully cyclized through cysteine–disulfide bond formation by air oxidation over 48 h without indications of intermolecular polymerized peptide precipitates. Both NODASA-H8 and NODASA-PH1 products were successfully purified (>95%) using semipreparative RP-HPLC as indicated by analytical HPLC analysis (Figure 2). LCMS analysis indicated that the desired peptide products were achieved (calculated M+2H: NODASA-H8 = 739.6, found 739.6; cyclized NODASA-PH1 = 760.6, found 760.6). LCMS chromatograms and mass spectra results acquired for the respective synthesis steps are provided in Figures S1–S5.

3.2 | Radio-HPLC Characterization

Radio-HPLC analysis showed that both peptides successfully incorporated ^{68}Ga, as indicated by the emerging [^{68}Ga]Ga-NODASA-H8 and [^{68}Ga]Ga-NODASA-PH1 radio peaks at $R_T = 6.69$ min and $R_T = 8.37$ min, respectively. The results are displayed in Figure 3. No additional emerging radio peaks were observed. The identity of both radiolabeled peptides was confirmed with complementary LCMS (UV 220 nm) analysis of nonradioactive Ga peptide reference compounds, indicating the correct mass and isotopic pattern (Figures S6 and S7, calculated M+2H: Ga-NODASA-H8 = 772.3, found 772.3; Ga-NODASA-PH1 = 793.3, found 793.2) and good R_T overlap with ^{68}Ga-radiolabeled counterparts. The small difference in R_T between the radiolabeled and nonradioactive reference compounds is a result of delay time between instrument detectors. No additional peaks or *m*/*z* signals were observed, indicating that a chemically pure metal conjugate was achieved.

3.3 | Evaluation of Labeling Parameters

Developing a new radiosynthesis method involves assessing radiolabeling parameters to ensure the reliable production of a radiolabeled product with the lowest possible ligand concentration and in the shortest amount of time. This process entails performing a series of reactions to evaluate radiolabeling outcomes based on various influencing parameters. These parameters include incubation temperature (ambient, 40°C, and 80°C) and incubation duration (5, 10, and 20 min), which were assessed on a series of radiolabeling reactions with different peptide concentrations (10, 25, 50, 75, and 100 μg/mL). The experimental pH value of 4.0 ± 0.5 was selected based on literature recommendations stating that pH levels between 3.0 and 5.0 are essential for NOTA-based gallium-68 radiolabeling [25, 34]. The radiolabeling performance was monitored by measuring the %RCY of the crude product using ITLC Method 1. The influence of temperature on %RCY was determined after an incubation time of 10 min, and the results are displayed in Figure 4. The influence of time on %RCY was determined at an incubation temperature of 80°C, and the results are displayed in Figure 5.

For both peptides, optimal labeling efficiencies were achieved at 80°C, with both peptides reaching %RCY > 95% at ≥ 25 μg/

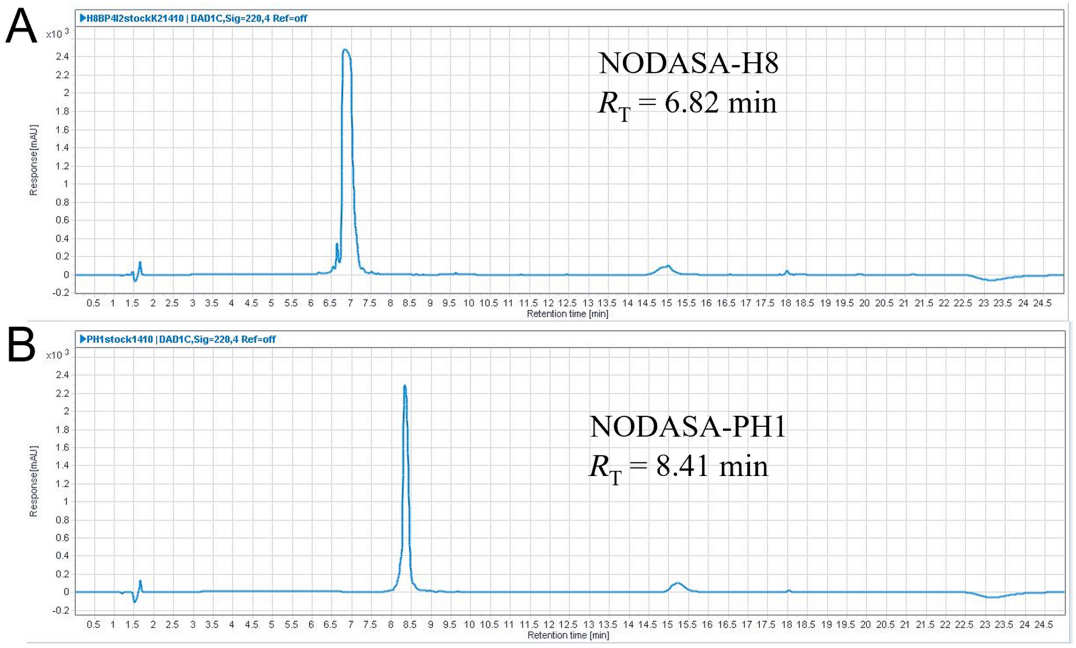

FIGURE 2 | Analytical HPLC (UV 220 nm) analysis of purified (A) NODASA-H8 and (B) cyclized NODASA-PH1.

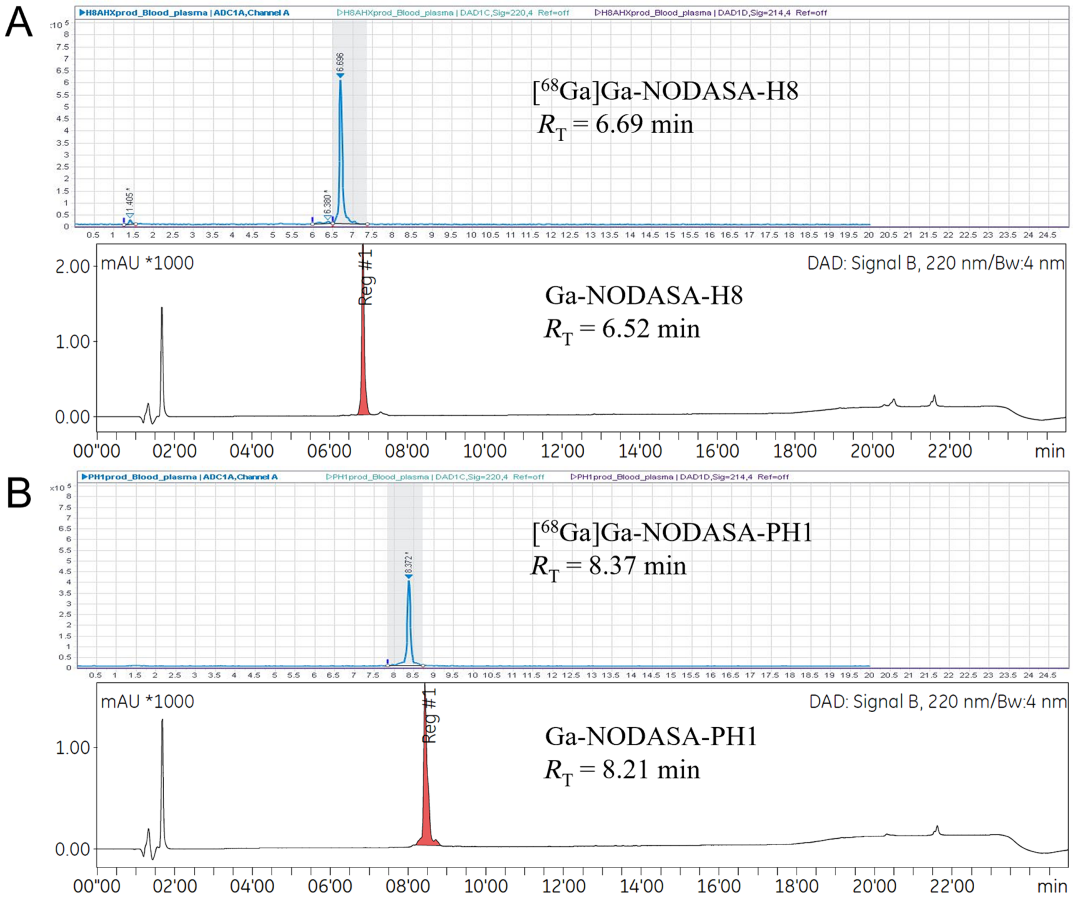

FIGURE 3 | Radio-HPLC characterization of [^{68}Ga] peptides and complementary LCMS characterization of nonradioactive Ga peptides. (A) Radiochromatogram (cps) of [^{68}Ga]Ga-NODASA-H8 (top) and UV (220 nm) chromatogram of Ga-NODASA-H8 (bottom) and (B) [^{68}Ga]Ga-NODASA-PH1 (top) and Ga-NODASA-PH1 (bottom). Good retention time overlap between radiolabeled [^{68}Ga] peptides and nonradioactive Ga peptide reference compounds. Radiolabeling reactions were performed with 100 μM peptide concentration at room temperature and analyzed using radio-HPLC Method 1.

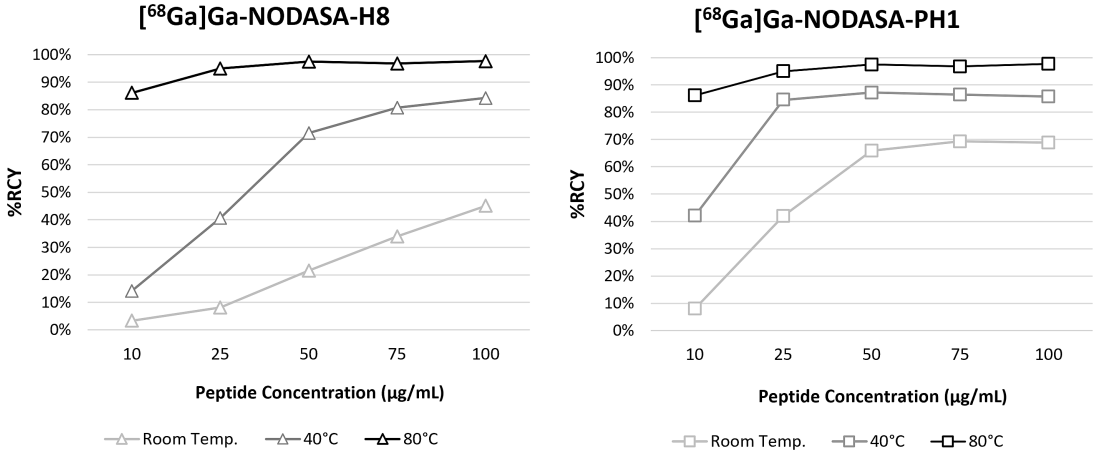

FIGURE 4 | Effect of temperature and on ^{68}Ga labeling for NODASA-conjugated peptides at a range of added peptide concentrations. Every data point represents an independent reaction. %RCY was determined using ITLC Method 1 (1.0 M ammonium acetate/methanol, 1:1) after an incubation time of 10 min.

mL (17 μM) within 10 min of incubation time. At ambient temperature and 40°C, NODASA-PH1 was able to chelate ^{68}Ga more efficiently than NODASA-H8, which is evident from the higher %RCY achieved at lower peptide concentrations. In terms of incubation duration, results indicate a clear increase in %RCY from 5 to 10 min when incubated at 80°C but then remaining unchanged. At lower concentrations (≤25 μg/mL), the benefit of extended incubation duration beyond 10 min is

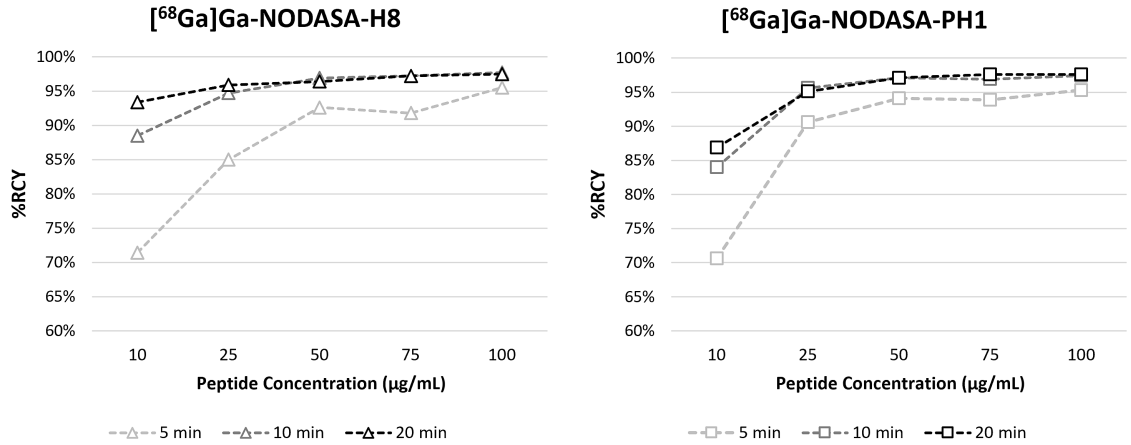

FIGURE 5 | Effect of incubation duration and on ^{68}Ga labeling for NODASA-conjugated peptides at a range of added peptide concentrations. Every data point represents an independent reaction incubated at 80°C. %RCY was determined using ITLC Method 1 (1.0 M ammonium acetate/methanol, 1:1).

more pronounced. It should be noted that while initial results indicated that both peptides achieved %RCY greater than 95% at ≥ 25 µg/mL within 10 min, subsequent radiolabeling reactions revealed that NODASA-H8 could be reliably radiolabeled quantitatively only at 75 µg/mL (data not shown). The reason for this variability is unclear, but it aligns with the more moderate radiolabeling performance observed for NODASA-H8 when compared to NODASA-PH1 at lower temperatures.

Because optimal %RCY was achieved at 80°C, the thermolytic stability of the peptide and radiometal conjugate was also assessed for up to 25 min with radio-HPLC to confirm the applicability of using higher temperatures. The results are displayed in Table 2. [^{68}Ga]Ga-NODASA-PH1 maintained chemical integrity and continuously chelated additional ^{68}Ga over time. On the other hand, [^{68}Ga]Ga-NODASA-H8 degradation could be observed at 25 min. Thus, radiolabeling [^{68}Ga]Ga-NODASA-H8 at high temperatures should be restricted to shorter reaction times.

3.4 | Optimized Radiosynthesis Protocol and Performance

Based on results from the evaluated radiolabeling, the following parameters were selected for routine radiolabeling: a ligand concentration of 25 µg/mL (17 µM) for [^{68}Ga]Ga-NODASA-H8 or 5.0 µg/mL (3.3 µM) for [^{68}Ga]Ga-NODASA-PH1. These concentrations are added to 1.0 mL of a pH 4.5 buffered ^{68}Ga eluate and incubated at 80°C for 10 min. It should be noted that, for the optimized method, reactions were performed in borosilicate glass vials provided by NTP Radioisotopes (Pelindaba, South Africa) instead of Eppendorf tubes. With borosilicate glass vials, quantitative labeling yields (>95% RCP) were more reliably achieved at a much lower ligand concentration for both peptides (e.g., from 75 to 25 µg/mL for [^{68}Ga]Ga-NODASA-H8 and from 25 to 5 µg/mL for [^{68}Ga]Ga-NODASA-PH1). This may be the result of a reduced adherence of peptide to the borosilicate glass surface in comparison to the plastic surfaces [39].

A C18-SPE method used for the purification of NOTA-based peptides was employed to eliminate excess buffer salts, unreacted free ^{68}Ga species, and ^{68}Ga colloids in order to produce a radiolabeled product suitable for in vitro and in vivo assays, experimental applications, or patient imaging [17, 40]. The presence of colloidal ^{68}Ga activity in the final product can negatively impact the available radiochemical yield and the quality and accuracy of PET images [41–43]. The C18-SPE method was successfully implemented, resulting in radiolabeled peptide products with a %RCP of over 98% (select examples of crude and SPE-purified radiolabeled products are shown in Figures S11 and S12). The C18-SPE cartridge was efficient in retaining the radiolabeled peptides during the loading and wash steps, effectively separating the unreacted free ^{68}Ga activity from the radiolabeled products. It was determined that at least 10% of EtOH/water (2.0 mL) solution is required to initiate the desorption of [^{68}Ga]Ga-NODASA-H8, while a minimum of 20% EtOH/water (2.0 mL) is needed for [^{68}Ga]Ga-NODASA-PH1. Quantitative desorption of either peptide was achieved using 50% EtOH/PBS (2.0 mL).

Next, key radiolabeling performance parameters such as %RCY, %RCP, product activity at the end of synthesis (EOS), and apparent molar activity (A_m) were calculated by performing consecutive radiosyntheses with the inclusion of SPE purification. Table 3 provides outcome of the repeatability of the radiosynthesis method by summarizing results gathered from consecutive preparations of [^{68}Ga]Ga-NODASA-PH1 and [^{68}Ga]Ga-NODASA-H8 using this radiosynthesis protocol. Robust production yields of radiochemically pure [^{68}Ga]Ga-NODASA-H8 and [^{68}Ga]Ga-NODASA-PH1 products suitable for further in vitro and in vivo applications were achieved [17, 40].

The interaction of labeled and unlabeled peptides with the same target binding site can hinder the accumulation of radiotracers, limiting the applicability of in vitro and in vivo assays that assess their viability. Thus, it is crucial to provide a radiotracer with a high molar activity when creating a target-specific radiotracer for PET imaging [44]. High levels of %RCY (at the end of synthesis) and molar activities were achieved within 42 min (post purification, without the inclusion of ethanol evaporation). Molar activities achieved for [^{68}Ga]Ga-NODASA-PH1 was similar to reported ^{68}Ga-radiolabeled NOTA-based chelator-functionalized

TABLE 2 | Determined radio-HPLC stability of peptide conjugates carried out at 80°C.

Peptide	80°C incubation time (min)	Integrated radio-HPLC peak area (%)		
		Intact ^{68}Ga peptide	Free ^{68}Ga	Degraded ^{68}Ga peptide
[^{68}Ga]Ga-NODASA-H8	5	90.90	9.06	nd
	25	86.40	5.98	7.32
[^{68}Ga]Ga-NODASA-PH1	5	96.46	3.54	nd
	25	98.63	1.37	nd

Abbreviation: nd, not detectable.

TABLE 3 | Radiolabeling features and outcome of the repetitive ^{68}Ga peptide radiolabeling performance.

Number of radiosynthesis (n)	[^{68}Ga]Ga-NODASA-H8 $n=8$	[^{68}Ga]Ga-NODASA-PH1 $n=7$
Generator elution		
^{68}Ga activity eluted (2.0-mL fraction)	612.4 ± 69.2 MBq	708.6 ± 35.8 MBq
Waste fraction (%)	8.1% ± 3.3%	5.7% ± 1.4%
Buffer solution	2.5-M sodium acetate	2.5-M sodium acetate
Radiolabeling reaction		
1.0-mL added activity (MBq)	180.4 ± 36.9 MBq	203.9 ± 12.5 MBq
Peptide concentration	25.0 μg/mL (16.7 μM)	5.0 μg/mL (3.3 μM)
Reaction temperature	80°C	80°C
Reaction time	10 min	10 min
Product crude RCP > 90%: n (%)[a]	8/8 (100%)	5/7 (71.4%)
Measured pH	4.0 ± 0.5	4.0 ± 0.5
Number of SPE purifications	$n=7$	$n=5$
SPE unit type	Waters SEP-PAK light C18 (130 mg)	
SPE elution mixture (v/v)	1:1 EtOH/PBS (2.0 mL)	
Crude RCP (%)[a]	96.7 ± 0.7	96.6 ± 1.7
Purified product RCP (%)[a]	99.7 ± 0.1	99.6 ± 0.2
Product activity at EOS (MBq)	96.7 ± 20.1	105.4 ± 9.2
Non–decay-corrected RCY (%)	55.6 ± 6.0	54.8 ± 2.4
Decay-corrected RCY (%)	91.2 ± 2.3	86.7 ± 4.0
A_m at EOS (GBq/μmol)	3.9 ± 0.8	34.0 ± 5.3
Total synthesis time (min)	41.3 ± 6.8	41.8 ± 5.6
SPE desorption (%)	93.7 ± 1.2	91.4 ± 2.5
Loss to apparatus including colloids (%)	8.6 ± 2.1	12.0 ± 3.2
Recovered activity (%)	99.8 ± 1.0	98.7 ± 1.3

[a]Radio-HPLC (Method 2) analysis was used.

peptides, such as [^{68}Ga]Ga-NOTA-UBI (13.8 ± 1.9 GBq/μmol) [33], [^{68}Ga]Ga-NOTA-RGD-GE11 (> 35.2 GBq/μmol) [45], and NODAGA-functionalized peptide heterodimer derivatives (25–61 GBq/μmol) [46]. Although a lower-than-usual molar activity was achieved for [^{68}Ga]Ga-NODASA-H8 compared to other NOTA-derived peptides, it is still comparable with other

radiotracers used in clinical practice [39]. The reason for the lower molar activity is unclear, but future experiments could explore modifications to the radiolabeling process, such as modifying pH, which was not assessed as part of the scope of this study.

We evaporated the ethanol content in the final radiolabeled product rather than dilute it to levels below 10% (as recommended for in vivo administration) [47] as high ethanol levels can directly influence radio-HPLC analysis in terms of ^{68}Ga peptide R_T and peak shape. Additionally, evaporation helped to concentrate the ^{68}Ga peptide activity to ensure a product suitable for future biological in vitro testing and small animal in vivo investigations. This approach also prevents ethanol from influencing LogP calculations and ensures the product's suitability for in vitro bacteriological assays.

3.5 | Radiochemical and Thermodynamic Stability Characterization

The development of a new radiosynthesis protocol involves carrying out a feasibility study to identify potential challenges for the compound's intended use. This includes evaluating the stability of the radiopharmaceutical product [17], a critical factor as it determines the timeframe within which a new radiotracer can be safely used for its intended purpose, for example, the tracer integrity from the time of labeling until it is administered to the patient. In addition, the radiometal–chelator complex should remain stable or irreversible in the presence of competitive chelating agents that mimic biologically occurring metal scavengers [48]. If radiometals such as ^{68}Ga are significantly released once injected into living species, it may result in nonspecific biodistribution, off-target pharmacology, or compromised PET image quality [49].

To assess its general stability, a sample of radiolabeled [^{68}Ga]Ga-NODASA-H8 and/-PH1 products were left in reaction solution (i.e., benchtop stability at pH 4.5) for 180 min and in PBS (pH 7.4) for 90 min followed by ITLC analysis (Method 1) to quantify any significant recurrence of free ^{68}Ga activity or ^{68}Ga colloids [17]. To assess the kinetic inertness of the radioconjugate, a transchelation challenge using up to 1000-fold molar excess of EDTA was applied for up to 90 min [50]. Potential ^{68}Ga release and EDTA transchelation were assessed using SG-ITLC (0.1 M citrate method). Transchelation of peptide-bound ^{68}Ga towards EDTA could be observed using this radio-ITLC method as free $^{68}Ga^{3+}$ and [^{68}Ga]Ga-EDTA shared similar R*f* values and are equally separated from radiolabeled peptides (Figure S10).

The outcomes of all three challenges are presented in Table 4. Both ^{68}Ga peptides exhibited a considerable degree of stability during the benchtop stability assessment, with only a minor reduction in [^{68}Ga]Ga-NODASA-PH1 integrity (~4%) observed after 180 min. Additionally, both compounds remained stable in PBS, as no significant changes in the integrity of the ^{68}Ga peptide were observed over a period of 90 min. These results suggest that the produced and formulated ^{68}Ga peptides are stable and reliable for in vitro and in vivo applications for at least 1.5 h post labeling. It is important to note that values greater than 100% can be attributed to continuous chelation occurring over time, resulting in a higher percentage of labeling within the challenge duration compared to the original radiolabeled product. Lastly, for both peptides, no substantial release and transchelation of ^{68}Ga activity were observed in the presence of EDTA over time, indicating the excellent kinetic stability of the radiometal–chelator complex.

3.6 | Physicochemical Characterization and Proteolytic Stability

To ensure optimal image quality in PET imaging, it is crucial that radiotracers, which are designed with high target specificity, remain stable in the bloodstream until they reach their intended target [49]. If a radiotracer is not stable due to premature degradation or metabolism in blood plasma, it can lead to the formation of fragments that exhibit altered biodistribution and nonspecific off-target binding, which can ultimately compromise PET image quality. Therefore, it is essential to maintain the stability of radiotracers in blood circulation to achieve accurate and reliable PET imaging results. Thus, the blood plasma enzymatic stability of [^{68}Ga]Ga-NODASA-H8 and [^{68}Ga]Ga-NODASA-PH1 was tested for up to 120 min to determine their clinical translation potential.

TABLE 4 | Stabilities for [^{68}Ga]Ga-NODASA-H8 and [^{68}Ga]Ga-NODASA-PH1 calculated from ITLC analysis.

	Normalized[a] percentage(%) of intact ^{68}Ga peptide						
Peptide	Incubation time (min)	Benchtop[b]	Incubation time (min)	PBS pH 7.4[b]	EDTA (50×)[c]	EDTA (100×)[c]	EDTA (1000×)[c]
[^{68}Ga]Ga-NODASA-H8[d]	30	100.7%	20	100.3%	94.3%	95.2%	95.0%
	60	100.7%	45	101.5%	94.3%	95.2%	95.0%
	180	100.2%	90	101.8%	94.5%	95.3%	94.6%
[^{68}Ga]Ga-NODASA-PH1[d]	30	100.6%	20	105.7%	91.0%	93.2%	92.8%
	60	100.5%	45	105.2%	89.8%	92.0%	91.8%
	180	96.2%	90	104.4%	91.5%	91.8%	91.4%

[a]Normalized to the %RCY of the crude product used for the experimental challenge, determined by ITLC analysis and peak quantification.
[b]Calculated using ITLC Method 1 (1.0 M ammonium acetate/methanol, 1:1).
[c]Calculated using ITLC Method 2 (0.1 M citrate, pH 5.0).
[d]^{68}Ga activity intervals used: benchtop (H8, 163–174 MBq; PH1, 159–171 MBq); PBS (H8, 48–53 MBq; PH1, 46–51 MBq); and EDTA challenges (H8, 48–53 MBq; PH1, 46–51 MBq).

Blood plasma stability results are displayed in Table 5, and comparative examples of radiochromatogram results for both radioconjugates between T_0 and T_{120} are displayed in Figure 6. No apparent change in %RCP were observed for [^{68}Ga]Ga-NODASA-PH1 up to 120 min. On the other hand, the majority of [^{68}Ga]Ga-NODASA-H8 degraded within 30 min. A complementary assay using nonradioactive Ga-NODASA-H8 and LCMS mass identification revealed that when scanning for an isotopic pattern of nonradioactive gallium, peptide cleavage occurs between histidine and serine (NODASA-Ahx-WH/SGTPHGGS-NH2, $m/z = 684.3$). The high stability of cyclic peptide [^{68}Ga]Ga-NODASA-PH1 as opposed to the linear peptide [^{68}Ga]Ga-NODASA-H8 may be expected. Some linear peptides are more prone to degradation by enzymes such as proteases or peptidases contained in blood plasma, and in that, cyclization of peptides is an established strategy to increase plasma stability. The high stability of [^{68}Ga]Ga-NODASA-PH1 (radioconjugate and molecular stability) indicates suitability for in vivo application, while application of [^{68}Ga]Ga-NODASA-H8 may be limited.

TABLE 5 | Observed plasma stability of radioconjugates determined by radio-HPLC (Method 1).

Serum stability	[^{68}Ga]Ga-NODASA-H8[a]	[^{68}Ga]Ga-NODASA-PH1[a]
Product %RCP	97.3%	99.8%
T_{5min}	89.4%	100.0%
T_{30min}	31.2%	100.0%
T_{60min}	20.0%	100.0%
T_{120min}	14.1%	100.0%

[a]Approximately 10 MBq of each ^{68}Ga peptide was utilized.

Key characteristics such as lipophilicity, polar surface area, and net charge play a crucial role in determining the radiotracer's

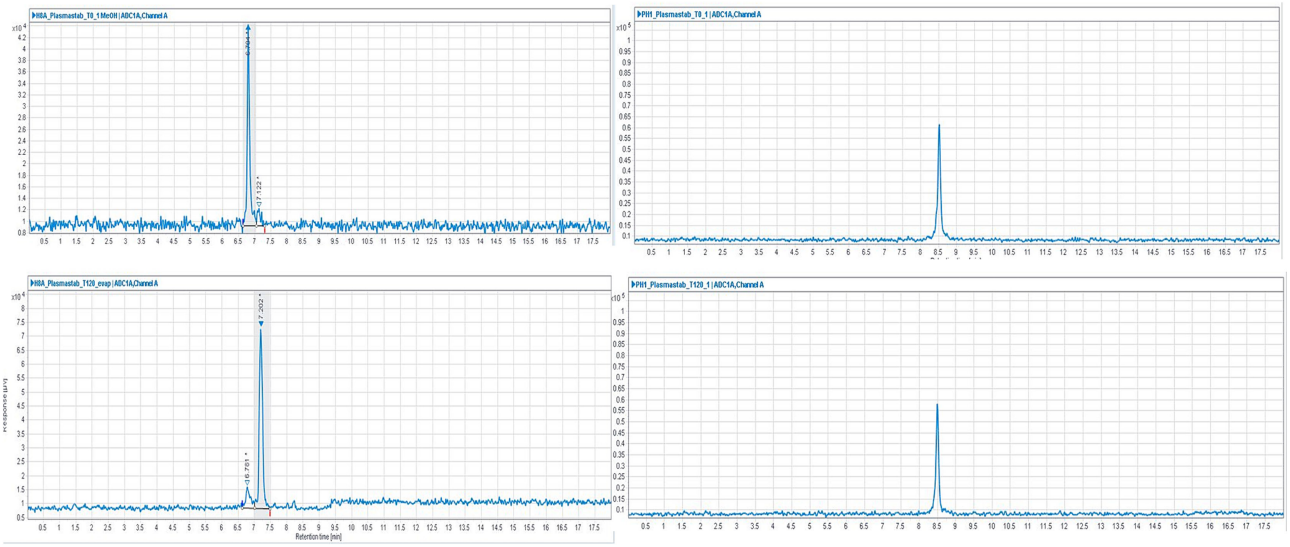

FIGURE 6 | Plasma stability radiochromatograms of [^{68}Ga]Ga-NODASA-H8 (left) and [^{68}Ga]Ga-NODASA-PH1 (right) obtained for T_0 (top) and T_{120} (bottom). At T_{120}, the majority of [^{68}Ga]Ga-NODASA-H8 degraded into a single radiolabeled by-product with a shifted retention time of 0.4 min (from 6.8 to 7.2 min).

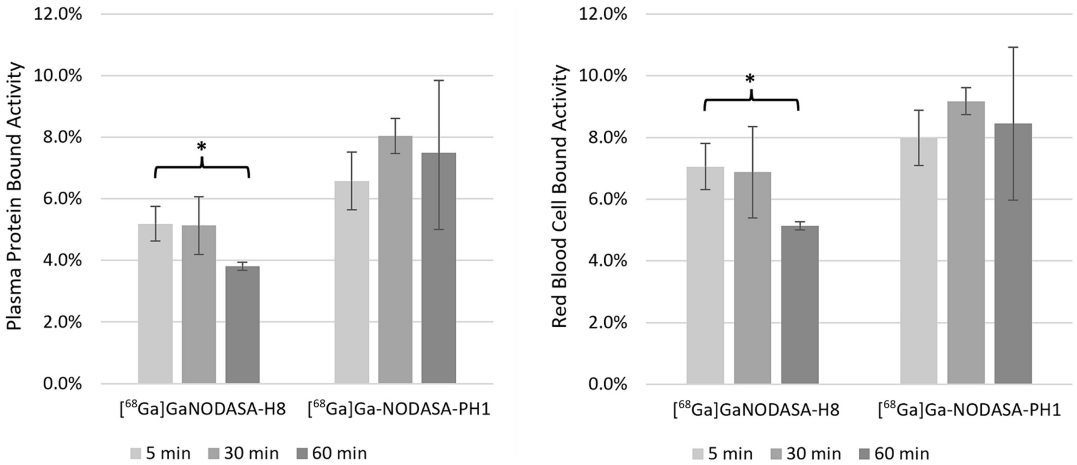

FIGURE 7 | Measured percentage of [^{68}Ga]Ga-NODASA-H8 and [^{68}Ga]Ga-NODASA-PH1 whole-blood cell binding (left) and plasma protein binding (right) up to 60-min incubation at 37°C. A two-tailed *t*-test indicated a significant decrease in blood cell and plasma protein–bound [^{68}Ga]Ga-NODASA-H8 over 60 min. *$p < 0.05$.

ability to cross the blood–brain barrier or reach tissues with active infections [51–53]. Highly lipophilic small molecules with high plasma protein binding often lead to slow clearance rates, while hydrophilic and positively charged radiotracers are eliminated quickly. Consequently, the degree of a compound's lipophilicity and its binding to blood cells and plasma proteins can predict its bioavailability and determine its potential for clinical application [54]. In this study, we quantified blood cell association, serum protein binding, and $LogD_{7.4}$ (lipophilicity) to assess the blood residence time.

Quantified blood distribution and plasma protein–binding results are displayed in Figure 7. Both [^{68}Ga]Ga-NODASA-H8 and [^{68}Ga]Ga-NODASA-PH1 showed low levels of blood cell and protein binding, indicating promising bioavailability when injected intravenously as a radiotracer. A significant decrease in both blood cell and protein-bound [^{68}Ga]Ga-NODASA-H8 activity was observed over 60 min ($p < 0.05$), while [^{68}Ga]Ga-NODASA-PH1 remained constant. This decrease over time may be the result of radiotracer degradation by-products that interact with blood cells and plasma protein to a lesser extent. These results are in line with the high hydrophilicity calculated for both [^{68}Ga]Ga-NODASA-H8 and [^{68}Ga]Ga-NODASA-PH1 ($LogP_{7.4} = -2.32 \pm 0.02$ and -2.50 ± 0.05, respectively). The degree of hydrophilicity is a surprising observation. While it is known that conjugation of biomolecules with macrocyclic bifunctional chelators such as NOTA and DOTA can increase hydrophilicity [55], a less hydrophilic compound was expected given that both peptide core sequences constitute a majority of hydrophobic amino acids (4/7 for H8 and 6/9 for PH1). This may ultimately be a factor that diminishes MTB targeting capability, given the hydrophobic nature of its cell walls. Additionally, the authors of peptide PH1 cited that target binding is most likely governed by hydrophobic interactions [24].

4 | Conclusion

The peptide syntheses, the development, the radiosynthesis performance, and a first-line in vitro assessment of pharmaceutical potential are presented for [^{68}Ga]Ga-NODASA-H8 and [^{68}Ga]Ga-NODASA-PH1. Each of the molecules comprised a previously approved MTB targeting phage display–generated peptide and NODASA as the functionalizing moiety for ^{68}Ga radiolabeling. The presented optimized radiosynthesis method can be used to reliably produce radiochemically pure products with sufficient activity yields suitable for future in vitro and in vivo application. Additionally, [^{68}Ga]Ga-NODASA-PH1 has high biological stability and favorable bioavailability, while [^{68}Ga]Ga-NODASA-H8 demonstrated compromised biological stability. The results presented herein are sufficient proof to enroll [^{68}Ga]Ga-NODASA-PH1 as the candidate PET radiotracer for further assessment, including bacterial uptake studies in vitro and mouse PET imaging studies, to assess MTB-derived infections noninvasively.

Acknowledgments

The authors would like to thank their funders, the National Research Foundation (NRF) of South Africa, University of KwaZulu-Natal College of Health Sciences (UKZN-CHS), and Nuclear Medicine Research Infrastructure (NuMeRI, NPC). The authors would also like to thank the Catalysis and Peptide Research Unit (CPRU), the South African Nuclear Energy Corporation (Necsa), the Pre-Clinical Imaging Facility (PCIF) staff, and the Steve Biko Academic Hospital, Department of Nuclear Medicine, University of Pretoria.

Conflicts of Interest

The authors declare no conflicts of interest.

Data Availability Statement

The data that support the findings of this study are available from the corresponding author upon reasonable request.

References

1. "Global Tuberculosis Report," World Health Organization, 2022, accessed August 5, 2024, https://www.who.int/teams/global-tuberculosis-programme/tb-reports/global-tuberculosis-report-2022.

2. C. J. L. Murray, K. S. Ikuta, F. Sharara, et al., "Global Burden of Bacterial Antimicrobial Resistance in 2019: A Systematic Analysis," *Lancet* 399, no. 10325 (2022): 629–655, https://doi.org/10.1016/S0140-6736(21)02724-0.

3. S. Annunziata, G. Treglia, F. Jamar, et al., "Nuclear Medicine Practice in the Field of Infection and Inflammation Imaging: A Pragmatical Survey," *European Journal of Nuclear Medicine and Molecular Imaging* 49, no. 7 (2022): 2113–2119, https://doi.org/10.1007/s00259-022-05725-9.

4. E. Dadachova and D. E. Rangel, "Highlights of the Latest Developments in Radiopharmaceuticals for Infection Imaging and Future Perspectives," *Frontiers in Medicine* 9 (2022): 819702.

5. J. P. Pijl, T. C. Kwee, R. Slart, and A. Glaudemans, "PET/CT Imaging for Personalized Management of Infectious Diseases," *Journal of Personalized Medicine* 11, no. 2 (2021): 133, https://doi.org/10.3390/jpm11020133.

6. G. B. Cross, J. O' Doherty, C. C. Chang, A. D. Kelleher, and N. I. Paton, "Does PET-CT Have a Role in the Evaluation of Tuberculosis Treatment in Phase 2 Clinical Trials?" *The Journal of Infectious Diseases* 229 (2023): 1229–1238, https://doi.org/10.1093/infdis/jiad425.

7. A. A. Ordonez, M. A. Sellmyer, G. Gowrishankar, et al., "Molecular Imaging of Bacterial Infections: Overcoming the Barriers to Clinical Translation," *Science Translational Medicine* 11, no. 508 (2019): eaax8251, https://doi.org/10.1126/scitranslmed.aax8251.

8. W. Wadsak and M. Mitterhauser, "Basics and Principles of Radiopharmaceuticals for PET/CT," *European Journal of Radiology* 73, no. 3 (2010): 461–469.

9. M. M. Alauddin, "Positron Emission Tomography (PET) imaging With (18)F-Based Radiotracers," *American Journal of Nuclear Medicine and Molecular Imaging* 2, no. 1 (2012): 55–76.

10. W. Chen and V. Dilsizian, "Molecular Imaging of Cardiovascular Device Infection: Targeting the Bacteria or the Host–Pathogen Immune Response?" *Journal of Nuclear Medicine* 61, no. 3 (2020): 319–326.

11. J. P. Pijl, P. H. Nienhuis, T. C. Kwee, A. W. Glaudemans, R. H. Slart, and L. C. Gormsen, "Limitations and Pitfalls of FDG-PET/CT in Infection and Inflammation," *Seminars in Nuclear Medicine* 51 (2021): 633–645.

12. A. Signore, F. Jamar, O. Israel, J. Buscombe, J. Martin-Comin, and E. Lazzeri, "Clinical Indications, Image Acquisition and Data Interpretation for White Blood Cells and Anti-Granulocyte Monoclonal Antibody Scintigraphy: An EANM Procedural Guideline," *European Journal of Nuclear Medicine and Molecular Imaging* 45, no. 10 (2018): 1816–1831, https://doi.org/10.1007/s00259-018-4052-x.

13. C. J. Palestro, A. Clark, E. E. Grady, et al., "Appropriate Use Criteria for the Use of Nuclear Medicine in Musculoskeletal Infection Imaging," *Journal of Nuclear Medicine* 62, no. 12 (2021): 1815–1831, https://doi.org/10.2967/jnumed.121.262579.

14. D. ten Hove, A. R. Wahadat, R. H. J. A. Slart, et al., "Added Value of Semi-Quantitative Analysis of [^{18}F]FDG PET/CT for the Diagnosis of Device-Related Infections in Patients With a Left Ventricular Assist Device," *European Heart Journal—Cardiovascular Imaging* 24 (2023): 819–828, https://doi.org/10.1093/ehjci/jeac260.

15. M. Hu, G. Chen, L. Luo, and L. Shang, "A Systematic Review and Meta-Analysis on the Accuracy of Fluorodeoxyglucose Positron Emission Tomography/Computerized Tomography for Diagnosing Periprosthetic Joint Infections," *Frontiers in Surgery* 9 (2022): 698781, https://doi.org/10.3389/fsurg.2022.698781.

16. O. Gordon, D. E. Lee, B. Liu, et al., "Dynamic PET-Facilitated Modeling and High-Dose Rifampin Regimens for *Staphylococcus aureus* Orthopedic Implant-Associated Infections," *Science Translational Medicine* 13, no. 622 (2021): eabl6851, https://doi.org/10.1126/scitranslmed.abl6851.

17. S. Alberto, A. A. Ordonez, C. Arjun, et al., "The Development and Validation of Radiopharmaceuticals Targeting Bacterial Infection," *Journal of Nuclear Medicine* 64, no. 11 (2023): 1676–1682, https://doi.org/10.2967/jnumed.123.265906.

18. A. C. Gouws, H. G. Kruger, O. Gheysens, et al., "Antibiotic-Derived Radiotracers for Positron Emission Tomography: Nuclear or "Unclear" Infection Imaging?" *Angewandte Chemie International Edition* 61, no. 45 (2022): e202204955.

19. E. W. Tucker, B. Guglieri-Lopez, A. A. Ordonez, et al., "Noninvasive ^{11}C-Rifampin Positron Emission Tomography Reveals Drug Biodistribution in Tuberculous Meningitis," *Science Translational Medicine* 10, no. 470 (2018): eaau0965, https://doi.org/10.1126/scitranslmed.aau0965.

20. A. A. Ordonez, H. Wang, G. Magombedze, et al., "Dynamic Imaging in Patients With Tuberculosis Reveals Heterogeneous Drug Exposures in Pulmonary Lesions," *Nature Medicine* 26, no. 4 (2020): 529–534, https://doi.org/10.1038/s41591-020-0770-2.

21. I. O. Lawal, S. Abubakar, A. O. Ankrah, and M. M. Sathekge, "Molecular Imaging of Tuberculosis," *Seminars in Nuclear Medicine* 53 (2022): 37–56.

22. J. Pande, M. M. Szewczyk, and A. K. Grover, "Phage Display: Concept, Innovations, Applications and Future," *Biotechnology Advances* 28, no. 6 (2010): 849–858, https://doi.org/10.1016/j.biotechadv.2010.07.004.

23. H. Yang, L. Qin, Y. Wang, et al., "Detection of *Mycobacterium tuberculosis* Based on H37Rv Binding Peptides Using Surface Functionalized Magnetic Microspheres Coupled With Quantum Dots—A Nano Detection Method for *Mycobacterium tuberculosis*," *International Journal of Nanomedicine* 10 (2014): 77–88.

24. N. A. Ngubane, L. Gresh, T. R. Ioerger, et al., "High-Throughput Sequencing Enhanced Phage Display Identifies Peptides That Bind Mycobacteria," *PLoS ONE* 8, no. 11 (2013): e77844.

25. M. I. Tsionou, C. E. Knapp, C. A. Foley, et al., "Comparison of Macrocyclic and Acyclic Chelators for Gallium-68 Radiolabelling," *RSC Advances* 7, no. 78 (2017): 49586–49599, https://doi.org/10.1039/C7RA09076E.

26. M. B. Mikulová and P. Mikuš, "Advances in Development of Radiometal Labeled Amino Acid-Based Compounds for Cancer Imaging and Diagnostics," *Pharmaceuticals* 14, no. 2 (2021): 167, https://doi.org/10.3390/ph14020167.

27. C. Decristoforo, R. D. Pickett, and A. Verbruggen, "Feasibility and Availability of ^{68}Ga-Labelled Peptides," *European Journal of Nuclear Medicine and Molecular Imaging* 39, no. Suppl 1 (2012): 31–S40, https://doi.org/10.1007/s00259-011-1988-5.

28. J. Dutta, P. K. Chinthakindi, P. I. Arvidsson, et al., "A Facile Synthesis of NODASA-Functionalized Peptide," *Synlett* 27, no. 11 (2016): 1685–1688.

29. C. A. Arbour, L. G. Mendoza, and J. L. Stockdill, "Recent Advances in the Synthesis of C-Terminally Modified Peptides," *Organic & Biomolecular Chemistry* 18, no. 37 (2020): 7253–7272, https://doi.org/10.1039/d0ob01417f.

30. I. Coin, M. Beyermann, and M. Bienert, "Solid-Phase Peptide Synthesis: From Standard Procedures to the Synthesis of Difficult Sequences," *Nature Protocols* 2, no. 12 (2007): 3247–3256, https://doi.org/10.1038/nprot.2007.454.

31. E. Calce, R. M. Vitale, A. Scaloni, P. Amodeo, and S. De Luca, "Air Oxidation Method Employed for the Disulfide Bond Formation of Natural and Synthetic Peptides," *Amino Acids* 47, no. 8 (2015): 1507–1515, https://doi.org/10.1007/s00726-015-1983-4.

32. D. D. Rossouw and W. A. Breeman, "Scaled-Up Radiolabelling of DOTATATE With ^{68}Ga Eluted From a SnO_2-Based ^{68}Ge/^{68}Ga Generator," *Applied Radiation and Isotopes* 70, no. 1 (2012): 171–175.

33. T. Ebenhan, N. Chadwick, M. M. Sathekge, et al., "Peptide Synthesis, Characterization and ^{68}Ga-Radiolabeling of NOTA-Conjugated Ubiquicidin Fragments for Prospective Infection Imaging With PET/CT," *Nuclear Medicine and Biology* 41, no. 5 (2014): 390–400, https://doi.org/10.1016/j.nucmedbio.2014.02.001.

34. D. Mueller, W. A. Breeman, I. Klette, et al., "Radiolabeling of DOTA-Like Conjugated Peptides With Generator-Produced ^{68}Ga and Using NaCl-Based Cationic Elution Method," *Nature Protocols* 11, no. 6 (2016): 1057–1066, https://doi.org/10.1038/nprot.2016.060.

35. J. Dutta, T. Naicker, T. Ebenhan, H. G. Kruger, P. I. Arvidsson, and T. Govender, "Synthetic Approaches to Radiochemical Probes for Imaging of Bacterial Infections," *European Journal of Medicinal Chemistry* 133 (2017): 287–308.

36. S. Shi, L. Zhang, Z. Wu, et al., "[^{68}Ga]Ga-HBED-CC-DiAsp: A New Renal Function Imaging Agent," *Nuclear Medicine and Biology* 82–83 (2020): 17–24, https://doi.org/10.1016/j.nucmedbio.2019.12.005.

37. Y. Xia, C. Zeng, Y. Zhao, X. Zhang, Z. Li, and Y. Chen, "Comparative Evaluation of ^{68}Ga-Labelled TATEs: The Impact of Chelators on Imaging," *EJNMMI Research* 10, no. 1 (2020): 36, https://doi.org/10.1186/s13550-020-00620-6.

38. A. H. Mdlophane, T. Ebenhan, B. Marjanovic-Painter, T. Govender, M. M. Sathekge, and J. R. Zeevaart, "Comparison of DOTA and NODAGA as Chelates for ^{68}Ga-Labelled CDP1 as Novel Infection PET Imaging Agents," *Journal of Radioanalytical and Nuclear Chemistry* 322, no. 2 (2019): 629–638, https://doi.org/10.1007/s10967-019-06693-5.

39. R. A. Davis, S. H. Hausner, and J. L. Sutcliffe, "Peptides as Radiopharmaceutical Vectors," in *Radiopharmaceutical Chemistry*, eds. J. S. Lewis, A. D. Windhorst, and B. M. Zeglis (Cham, Switzerland: Springer International Publishing, 2019), 137–162.

40. A. Signore, V. Bentivoglio, M. Varani, and C. Lauri, "Current Status of SPECT Radiopharmaceuticals for Specific Bacteria Imaging," *Seminars in Nuclear Medicine* 53 (2023): 142–151, https://doi.org/10.1053/j.semnuclmed.2022.12.001.

41. M. Petrik, A. Vlckova, Z. Novy, L. Urbanek, H. Haas, and C. Decristoforo, "Selected ^{68}Ga-Siderophores Versus ^{68}Ga-Colloid and ^{68}Ga-Citrate: Biodistribution and Small Animal Imaging in Mice," *Biomedical Papers of the Medical Faculty of the University Palacky, Olomouc, Czech Republic* 159, no. 1 (2015): 60–66, https://doi.org/10.5507/bp.2014.052.

42. B. J. B. Nelson, J. D. Andersson, F. Wuest, and S. Spreckelmeyer, "Good Practices for ^{68}Ga Radiopharmaceutical Production," *EJNMMI Radiopharmacy and Chemistry* 7, no. 1 (2022): 27, https://doi.org/10.1186/s41181-022-00180-1.

43. M. Meisenheimer, Y. Saenko, and E. Eppard, *Gallium-68: Radiolabeling of Radiopharmaceuticals for PET Imaging—A Lot to Consider* (London, UK: IntechOpen, 2021).

44. G. Luurtsema, V. Pichler, S. Bongarzone, et al., "EANM Guideline for Harmonisation on Molar Activity or Specific Activity of Radiopharmaceuticals: Impact on Safety and Imaging Quality," *EJNMMI Radiopharmacy and Chemistry* 6, no. 1 (2021): 34, https://doi.org/10.1186/s41181-021-00149-6.

45. C. J. Chen, C. H. Chan, K. L. Lin, et al., "^{68}Ga-Labelled NOTA-RGD-GE11 Peptide for Dual Integrin and EGFR-Targeted Tumour Imaging," *Nuclear Medicine and Biology* 68–69 (2019): 22–30, https://doi.org/10.1016/j.nucmedbio.2018.11.003.

46. S. Lindner, L. Fiedler, B. Wängler, P. Bartenstein, R. Schirrmacher, and C. Wängler, "Design, Synthesis and In Vitro Evaluation of Heterobivalent Peptidic Radioligands Targeting Both GRP- and VPAC1-Receptors Concomitantly Overexpressed on Various Malignancies—Is the Concept Feasible?" *European Journal of Medicinal Chemistry* 155 (2018): 84–95, https://doi.org/10.1016/j.ejmech.2018.05.047.

47. K. Serdons, A. Verbruggen, and G. Bormans, "The Presence of Ethanol in Radiopharmaceutical Injections," *Journal of Nuclear Medicine* 49, no. 12 (2008): 2071, https://doi.org/10.2967/jnumed.108.057026.

48. E. W. Price and C. Orvig, "Matching Chelators to Radiometals for Radiopharmaceuticals," *Chemical Society Reviews* 43, no. 1 (2014): 260–290, https://doi.org/10.1039/C3CS60304K.

49. F. Mota, A. A. Ordonez, G. Firth, C. A. Ruiz-Bedoya, M. T. Ma, and S. K. Jain, "Radiotracer Development for Bacterial Imaging," *Journal of Medicinal Chemistry* 63, no. 5 (2020): 1964–1977, https://doi.org/10.1021/acs.jmedchem.9b01623.

50. Y. Zhang, M. Hao, L. Li, et al., "Research Progress of Contrast Agents for Bacterial Infection Imaging In Vivo," *TrAC Trends in Analytical Chemistry* 159 (2023): 116916, https://doi.org/10.1016/j.trac.2023.116916.

51. V. Patamia, C. Zagni, I. Brullo, et al., "Computer-Assisted Design of Peptide-Based Radiotracers," *International Journal of Molecular Sciences* 24, no. 7 (2023): 6856, https://doi.org/10.3390/ijms24076856.

52. J. Kleynhans, H. G. Kruger, T. Cloete, J. R. Zeevaart, and T. Ebenhan, "In Silico Modelling in the Development of Novel Radiolabelled Peptide Probes," *Current Medicinal Chemistry* 27, no. 41 (2020): 7048–7063, https://doi.org/10.2174/0929867327666200504082256.

53. J. Kleynhans, A. F. Grobler, T. Ebenhan, M. M. Sathekge, and J. R. Zeevaart, "Radiopharmaceutical Enhancement by Drug Delivery Systems: A Review," *Journal of Controlled Release* 287 (2018): 177–193, https://doi.org/10.1016/j.jconrel.2018.08.008.

54. J. Bolcaen, J. Kleynhans, S. Nair, et al., "A Perspective on the Radiopharmaceutical Requirements for Imaging and Therapy of Glioblastoma," *Theranostics* 11, no. 16 (2021): 7911–7947, https://doi.org/10.7150/thno.56639.

55. J. D. Northrup, R. H. Mach, and M. A. Sellmyer, "Radiochemical Approaches to Imaging Bacterial Infections: Intracellular Versus Extracellular Targets," *International Journal of Molecular Sciences* 20, no. 22 (2019): 5808, https://doi.org/10.3390/ijms20225808.

Supporting Information

Additional supporting information can be found online in the Supporting Information section.